Nagata Koh - ichi (Orcid ID: 0000-0002-6827-8434)

MED13L and its disease-associated variants influence the dendritic development of cerebral cortical neurons in the mammalian brain

Nanako Hamada[1], Ikuko Iwamoto[1] and Koh-ichi Nagata[1,2]

[1]*Department of Molecular Neurobiology, Institute for Developmental Research, Aichi Developmental Disability Center, 713-8 Kamiya, Kasugai, Aichi 480-0392, Japan*

[2]*Department of Neurochemistry, Nagoya University Graduate School of Medicine, 65 Tsurumai-cho, Showa-ku, Nagoya, Aichi 466-8550, Japan*

Correspondence;

Koh-ichi Nagata

Department of Molecular Neurobiology

Institute for Developmental Research, Aichi Developmental Disability Center

713-8 Kamiya, Kasugai 480-0392, Japan

Tel; (81)-568-88-0811 Fax; (81)-568-88-0829 e-mail; knagata@inst-hsc.jp

Key words: Mediator complex, MED13L, pathogenic variations, cortical neuron, dendrite

List of abbreviations: ID, intellectual disability; MED13L, Mediator Complex Subunit 13 like; RRID, Research Resource Identifier (see scicrunch.org); TGA, transposition of the great arteries; SNP, Single Nucleotide Polymorphisms; VZ, ventricular zone; TGFβ, transforming growth factor β; KO, knockout.

Abstract

The Mediator complex comprises multiple subcellular subunits that collectively function as a molecular interface between RNA polymerase II and gene-specific transcription factors. Recently, genetic variants to one subunit of the complex, known as MED13L (Mediator Complex Subunit 13 like), has been implicated in syndromic intellectual disability and distinct facial features, frequently accompanied by congenital heart defects. We investigated the impact of 5 disease-associated *MED13L* variants on the subcellular localization and biochemical stability of MED13L protein *in vitro* as well as *in vivo*. In overexpression assays using cortical neurons from embryonic mouse cerebral cortices transduced by *in utero* electroporation-mediated gene transfer, we found that mouse orthologues of human MED13L-p.P866L and -p.T2162M missense variants accumulated in the nucleus, while the p.S2163L and p.S2177Y variants were diffusely distributed in the cytoplasm. In contrast, we found that the p.Q1922* truncation variant barely detectable in transduced cells, a phenotype reminiscent of this variant that results in *MED13L* haploinsufficiency in humans. Next, we analyzed these variants for their effects on neuronal migration, dendritic growth, spine morphology, and axon elongation of cortical neurons *in vivo*. There, we found that overexpression of the p.P866L variant resulted in reduced number and length of dendrites of cortical layer II/III pyramidal neurons. Furthermore, we show that mMED13L-knockdown abrogated dendritic growth *in vivo*, and this effect was significantly rescued by co-electroporation of an RNAi-resistant mMED13L, but weakly by the p.T2162M variant, and not at all by the p.S2163L variant. However, overexpression of the p.S2163L variant inhibited mature dendritic spine formation *in vivo*. Expression of each of the 5 variants did not affect neuronal cell migration and callosal axon elongation *in vivo*. Taken

together, our results demonstrate that MED13L expression is relevant to corticogenesis and influences the dendritic branching characteristics of cortical excitatory neurons. Our study also suggests that disease-associated *MED13L* variants may directly cause morphological and functional defects in cortical neurons in different ways.

Introduction

MED13L, encoded by the Mediator complex subunit 13-like (*MED13L*) gene, is a subunit of the Mediator complex, which functions as a large transcriptional coactivator assembly (Taatjes 2010; Malik and Roeder 2010). It is recognized that the Mediator complex is evolutionarily conserved and ubiquitously expressed (Casamassimi and Napoli 2007), and is composed of 4 distinct modules (head, middle, tail and CDK8 kinase modules), among which the kinase module includes 1 of these 2 proteins, MED13 or MED13L (Pescosolido *et al.* 2013; Bulayeva *et al.* 2015). This complex is thought to function as a transcriptional regulator for most RNA polymerase II-transcribed genes (Casamassimi and Napoli 2007; Liu *et al.* 2013), by acting as a molecular bridge between transcription factors bound at upstream DNA regulatory elements and the transcription machinery (Malik and Roeder 2010).

The roles for Mediator complex in neuronal development is reflected in the finding that genetic abnormalities of various subunits lead to human neurological conditions. For example, variations to the following genes are associated with clinical conditions, as follows: *MED15* in DiGeorge syndrome (Berti *et al.* 2001), *MED25* in Charcot–Marie–Tooth neuropathy (Leal *et al.* 2009), *MED13* (Boutry-Kryza *et al.* 2012) and *MED23* (Hashimoto *et al.* 2011) in intellectual disability (ID), *MED17* in infantile cerebral and cerebellar atrophy (Kaufmann *et al.* 2010), and *MED12* in X-linked genetic disorders, Opitz–Kaveggia syndrome (Risheg *et al.* 2007) and Lujan–Fryns syndrome (Schwartz *et al.* 2007). As for *MED13L*, a chromosomal balanced translocation disrupting the gene was first reported in a patient diagnosed with transposition of the great arteries (TGA) and ID (Muncke *et al.* 2003). Since this discovery, further genetic abnormalities that disrupt *MED13L* have been reported, including intragenic or

whole gene deletions, duplications, chromosomal translocations, as well as *de novo* frameshift/nonsense/splice site variations. Such *MED13L* genetic variants have been detected in individuals with ID and developmental delay that are comorbid with dysmorphic features and congenital heart defects (Asadollahi *et al.* 2013; Adegbola *et al.* 2015; Cafiero *et al.* 2015; van Haelst *et al.* 2015; Yamamoto *et al.* 2017; Gordon *et al.* 2018; Tørring *et al.* 2019). While current genetic and clinical findings indicate that *MED13L* is a haploinsufficient gene (Yamamoto *et al.* 2017) essential to brain development, yet the biological roles for MED13L and its disease-associated variants remain to be elucidated, particularly in cells of the nervous system. To address this, we recently reported that MED13L is widely expressed in mammalian cortical neurons during brain development (Hamada *et al.* 2021b). Furthermore, we found that MED13L can be localized to excitatory synapses of primary cultured mouse hippocampal neurons (Hamada *et al.* 2021b).

Here, we carried out a series of *in vitro* and *in vivo* studies using a mouse model to clarify the neurodevelopmental roles for MED13L and its disease-associated variants in cells of the mammalian cerebral cortex. We found that MED13L plays an essential role in brain development through the regulation of dendritic arborization and synapse formation by cortical neurons. Furthermore, we characterized 5 disease-associated variants, 3 of which (p.P866L, p.S2163L, and p.S2177Y) are associated with ID and autistic features and seizures; as well as 2 additional variants (p.T2162M and p.Q1922*) associated with ID (Smol *et al.* 2018). From these studies, we find that disease-associated *MED13L* variants influence the development of cerebral cortex neurons in different ways. Together, our findings improve our understanding of

how genetic variations to *MED13L* influence neuronal development and underlie brain development and disease.

2. Materials and Methods

2.1 Ethics statement

This work adheres to guidelines for animal experiments and related activities within our academic research institution, under the jurisdiction of the Ministry of Education, Culture, Sports, Science and Technology, Japan. All protocols for animal handling and treatment were reviewed and approved by the animal care and use committee of Institute for Developmental Research, Aichi Developmental Disability Center (approval number; 2019-013). The study was not pre-registered.

2.2 Animals

Pregnant ICR mice (hybrid strain originally derived from Jcl:ICR strain) (RRID:IMSR_TAC:icr), weighing between 250-300 g, were obtained from Japan SLC Inc. (Shizuoka, Japan) (http://www.jslc.co.jp/animals/mouse.php#mouse-cat-05). Mice were housed (one animal in each cage) with 12-to-12 h-light-dark cycle, humidity (60 ± 5 %), with access to food and water *ad libitum* in individually ventilated cages. A total of 115 animals were used in this study. Analyses of neuronal migration and differentiation *in vivo* with acute knockdown were carried out ($n \geq 3$ animals/group) based on a previous study (Hamada *et al.* 2018). Neither the sample size nor the exclusion criteria were predetermined in this study. When sacrificed, mice were euthanized by cervical dislocation using a protocol previously described to minimize pain and suffering (Roustan *et al.* 2012).

2.3 Plasmids

Mouse (m)MED13L cDNA was cloned by PCR from mouse brain cDNA pools and constructed into pCAG-Myc provided by Dr. T. Kawauchi (Kyoto Univ., Japan) or pCAG-GFP vector (catalogue #11150, Addgene Inc., Cambridge, MA). pCAG-M-Cre was kind gifts from S. Miyagawa (Osaka Univ., Japan). pCALNL(loxP-neomycin-loxP)-GFP was made from pCALNL-DsRed (RRID:Addgene_13769, Addgene Inc.). pSuper-puro RNAi vector (OligoEngine, Seattle, WA) was designed to target 2 distinct coding sequences in mMED13L cDNA (pSuper-mMED13L#1: 5'-GATCAACGAGGAACACTTA-3', nt573-591; pSuper-mMED13L#2: 5'-CTAACAAGCGGTTCAAAAT -3', nt2012-2030). Numbers indicate the position from transcription start sites. pSuper-H1.shLuc designed against luciferase (5'-CGTACGCGGAATACTTCGA-3') was used as a control RNAi vector. To generate an RNAi-resistant mMED13L (mMED13L-R), 4 mutations were introduced as synonymous mutations to the polypeptide coding sequence targeted by pSuper-mMED13L#1 (5'-GATCAATGAAGAGGCATTTA-3'). The variants mMED13L-P866L, -T2159M, -S2160L, -S2174Y and -Q1919*, which are orthologous in sequence alignment with human MED13L-P866L, -T2162M, -S2163L, -S2177Y and -Q1922*, were all made using a KOD-Plus Mutagenesis kit (Toyobo, Osaka, Japan) with mMED13L-R as a template, and constructed into the pCAG-Myc vector. We refer to mMED13L-P866L, -T2159M, -S2160L, -S2174Y, and -Q1919* as mMED13L-PL, -TM, -SL, -SY and -Q*, respectively, in this study. Also, cDNA sequences for mMED13L-R2149Q and -I2203V, orthologous to sequences for human MED13L-R2152Q and -I2206V (Single Nucleotide Polymorphism in healthy individuals),

respectively, were also cloned into pCAG-Myc, and termed mMED13L-RQ(SNP) and -IV(SNP). All constructs were verified by DNA sequencing.

2.4 Cell culture, transfection, western blotting and immunofluorescence

COS7 (*Cercopithecus aethiops* kidney) cell line, which is not listed as a commonly misidentified cell line by the International Cell Line Authentication Committee, was obtained from American Type Culture Collection (RRID: CVCL_0224) and used for 10-15 passages before discard. This cell line was chosen because of its utility for overexpression studies. We have not authenticated the cell line since its purchase. Primary mouse cortical neurons and COS7 cells were cultured essentially as previously described (Hamada *et al.* 2021b). Primary cultures of mouse neurons were prepared as follows: for a batch of cells, a pregnant mouse was used per cell culture, and first deeply anesthetized with a mixture of medetomidine (0.75 mg/kg), midazolam (4 mg/kg), and butorphanol (5 mg/kg) (Kawai *et al.* 2011). The cortices of E16 embryonic mice were dissected, collected in Hanks' balance salt solution, and minced. After incubation in trypsin-EDTA, neurons were triturated in Neurobasal medium (Invitrogen, Carlsbad, CA) supplemented with 2% B-27 supplement (Invitrogen), 0.5% L-glutamine solution (Cell Science & Technology Institute, Miyagi, Japan), 100 U/ml penicillin and 100 μg/ml streptomycin (Invitrogen). Neurons were then cultured in Neurobasal medium with B27, 1 mM L-glutamine, and penicillin/streptomycin. Transient transfections were carried out with PEImax reagent according to the manufacturer's instructions (Polysciences, Warrington, PA). Protein concentration was determined with a micro bicinchoninic acid protein assay reagent kit (Thermo Fisher Scientific, Rockford, IL). Western blotting and immunofluorescence analyses were carried out as described previously (Hamada *et al.* 2021a). Polyclonal rabbit anti-MED13L and

anti-Sept11 antibodies were generated as described previously (Hanai *et al.* 2004; Hamada *et al.* 2021b). Monoclonal anti-Myc and -β-actin antibodies from Cell Signaling Technology (Cat# 2276, RRID: AB_331783, and Cat# 3700, RRID: AB_2242334) were used (Danvers, MA). Alexa Fluor® 488-, 568- and 647-labeled IgG were used as secondary antibodies (Abcam, Tokyo, Japan, Cat# ab150077, RRID: AB_2630356; Cat# ab175471, RRID: AB_2576207, and Cat# ab150075, RRID: AB_2752244). 4', 6-diamidino-2-phenylindole (DAPI; Nichirei Bioscience, Tokyo, Japan) was used for staining DNA. Fluorescent images were captured using an LSM-880 confocal laser microscope (Carl Zeiss, Oberkochen, Germany).

2.5 *In utero* electroporation

Pregnant ICR mice provided by Japan SLC (Shizuoka, Japan) were first anesthetized with an injection of a cocktail of three drugs, as mentioned above. *In utero* electroporation was then conducted as described previously (Tabata and Nakajima 2001; Hamada *et al.* 2016). Briefly, pCAG expression and RNAi vectors were injected into the lateral ventricle of embryos using a glass micropipette made from a microcapillary tube (GD-1; Narishige, Tokyo, Japan). Then, each embryo was placed between a tweezers-type disc electrode (5 mm in diameter) (CUY650-5; NEPA Gene, Chiba, Japan) and subjected to 5 electronic pulses (50 ms of 35 V) at 450 ms intervals using an electroporator (NEPA21; NEPA Gene). In this method, plasmids are introduced into the somatosensory area of the embryonic cortex which is included in the parietal lobe. On collection, dissected brains were fixed at indicated postnatal days, sectioned, and then analyzed. All experimental procedures were carried out in the daytime. Animals were neither selectively excluded nor had inadvertently died before collection during experimentation. A graphical time-line of the study design is shown in Supplementary Fig.1.

2.6 Quantitative analysis of neuronal migration and axon elongation

Three electroporated brains from different dams were used for each experiment. To quantify neuronal migration *in vivo*, the distribution of GFP-positive cortical cells in brain slices was quantified by 2-dimensional densitometric scans for GFP fluorescence intensity. The laminar distribution of GFP-labeled neurons across cortical layers was analyzed with ImageJ software according to the user manual. To quantify callosal axon growth at P7, the GFP signal intensity of axons was measured in a 170 x 300 μm rectangle on both the ipsilateral (before entering the corpus callosum (CC)) (yellow) and contralateral (after leaving the CC) (green) positions indicated in Supplementary Fig. 3B. We then calculated the ratio of the contralateral signal intensity to that of the corresponding ipsilateral side using ImageJ software. To estimate axon growth by electroporated cells at E17, the axonal GFP intensity in a square region (green) was normalized to the total GFP intensity (white) indicated in Supplementary Figure 2B using ImageJ software.

2.7 Quantitative analysis of dendritic arbor formation

To measure the lengths and numbers of dendrites on post-migratory (mature) neurons, images of GFP-positive neurons in the layer II-III of cerebral cortex at P7 and P30 were acquired by confocal microscopy. Image J software was then used to quantify dendritic length. Branch points of dendrites were analyzed by Sholl analysis.

2.8 Quantitative analysis of spine morphologies

Transfected neurons were immunostained with anti-GFP and chosen arbitarily. For morphology analyses, a series of 0.2-μm z-stacks was captured using an LSM-880 confocal laser microscope in order to generate image projections so as to obtain a composite images. For dendritic spine

analyses, spines were defined as protrusions with a range of 0.2 to 4 μm in length, with or without a spine head. Dendritic spine densities were measured by counting the number of protrusions per 10 μm-length of primary dendrites. Spine density was first averaged per neuron, following which the mean densities from multiple individual neurons were calculated. Morphological assessments of spine density and shape were performed by Imaris software (Carl Zeiss).

2.9 Statistical analysis

For all cell imaging experiments, cell counting and traces were assessed in a blinded manner by technical staff who was not aware of the experimental conditions. Results are expressed as means ± SE. Neither randomization nor sample size calculations was performed in this study. Sample sizes were instead determined as described (Matsumura *et al.* 2020), with 3-8 animals used, as previously described (Hamada *et al.* 2018). Where data was obtained from only 2 groups, a Welch's *t*-test was used for statistical comparison. For data obtained from more than 3 groups, a one-way analysis of variance (ANOVA) was performed, followed by a Tukey-Kramer least significant difference test (LSD) to absolute values as a *post hoc* test of multiple comparisons. The level of statistical significance was set at $p<0.05$. Statistical analysis was performed using Prism software (GraphPad Software Inc., CA). Data were not assessed for normality in this study. No test for outliers was conducted in this study. Because data were not assessed for normality, we did not describe and justify any normalization, which did not result in the need for non-parametric analysis.

2.10 Availability of Data and Materials

Custom-made materials described in this study as well as data will be shared upon reasonable request. The datasets used and/or analyzed during the current study are available from the corresponding author on reasonable request.

Results

Disruptions to mMED13L influence dendritic development *in vivo*

To explore the possibility that MED13L influences neuronal development and synaptic functions, we first examined the effects of *mMED13L*-knockdown on the development of dendrites on cortical neurons *in vivo*. To achieve this, we designed 2 distinct RNAi vectors, pSuper-mMED13L#1(sh-mMED13L#1) and #2, each targeting distinct sequences within the coding sequence. Each vector efficiently silenced mMED13L as evaluated in overexpression studies with COS7 cells (Fig. 1A). In addition, we generated a version of mMED13L that is refractory to RNAi-mediated knockdown, designated as mMED13L-R, and confirmed its resistance to sh-mMED13L#1 suppression in COS7 cells (Fig. 1A). We performed immunostaining for endogenous mMED13L signal to confirm RNAi-mediated knockdown , as observed when staining the nuclei of primary cultured cortical neurons following shRNA treatment *in vitro,* as shown (Fig. 1B). Next, we electroporated VZ cells of the E14.5 embryonic mouse cortex with sh-mMED13L#1 or #2 and studied the effect of these genetic manipulations 7 days after electroporated mice were born (P7). As shown, we found that the dendritic arborization of excitatory neurons in layer II/III at P7 was dramatically affected by *mMED13L* RNAi, observed as a significant decrease in apical dendritic length following treatment with sh#1 or sh#2 (Fig. 1C and D). Significantly, we performed rescue experiments to find that the

dendritic length phenotype documented following sh-mMED13L#1 treatment was corrected by co-expression of mMED13L-R, thereby demonstrating a cell-autonomous effect and ruling out non-specific effects of RNAi on dendritic arborization (Fig. 1C and D). While quantification analyses revealed that, compared to control treatment, mMED13L-knockdown suppressed both apical and basal dendrite development, the effect on arborization of basal dendrites was impaired more severe (Fig. 1D). We also performed Sholl analyses and identified a significant decrease in the numbers of dendritic branch points in mMED13L-deficient neurons (Fig. 1E). Notably, this phenotype was partially rescued by co-treatment with mMED13L-R in a statistically significant manner (Fig. 1E).

Next, we examined the long-term effects of mMED13L-knockdown on the dendritic arborization of cortical neurons within adult (P30) mouse brains. To do this, we performed high-power confocal image reconstructions of GFP-labelled neurons and documented the number and total length of basal dendrites on representative neurons from each treatment group. Apical dendrites were excluded from the quantification analyses owing to methodological constraints that limit our ability to study the main apical dendrite shaft of P30 neurons, as it frequently does not fit the 3D-analytical area examined during data-capture, thereby leading to inaccurate measurements of apical dendritic length and branch points. Nevertheless, our quantification studies show that the dendritic arborization of mMED13L-deficient neurons was significantly decreased, compared to control cells (Fig. 2A and B). Our results from Sholl analysis of neurons also demonstrate that dendritic complexity is significantly reduced in mMED13L#1shRNA-treated neurons compared to control (Fig. 2C). Taken together with our results on P7 neurons, these findings indicate that mMED13L knockdown leads to a

suppression, rather than a delay in the dendritic arborization of cortical neurons. Collectively, we concluded that mMED13L is possible to be essential for dendritic arbor development during corticogenesis and its deficiency may impair postnatal neuronal network formation. The phenotypes in acute knockdown experiments are considered to mimic the pathophysiological conditions of *MED13L* haploinsufficiency.

Given the effects of knockdown on dendritic development, we wanted to investigate whether mMED13L was involved in the positioning of newly generated cortical neurons. To this end, we performed *in utero* electroporations to introduce pSuper-H1.shLuc (control), sh-mMED13L #1 or #2 expression vectors together with pCAG-GFP to identify labelled cells lying within the embryonic cortical VZ of E14.5 mouse embryos. Following electroporation, brains were harvested and analyzed by cryosectioning and immunofluorescence microscopy at E17.5 and P2. In these studies, we found that treatment with mMED13L shRNAs did not significantly affect the distribution of GFP-labelled cortical cells distributed within the upper layers of the E17.5 cortex (Supplementary Fig. 2A) or in layers II-III of the P2 cortex (Supplementary Fig. 3A). Furthermore, we analyzed the effects of mMED13L-knockdown on axon elongation *in vivo*. As shown, we found that knockdown of mMED13L in E14.5 cortical cells did not influence axon outgrowth of GFP-electroporated cells analyzed at E17.5 as well as P7, with axons also found to be extending contralateral projections in a manner that was not significantly different to control treatment (Supplementary Fig. 2B and Supplementary Fig. 3B) as well as in P16 mice (data not shown). Thus, we find that MED13L knockdown did not significantly influence cortical cell positioning and axon outgrowth in the developing and postnatal mouse cortex.

Characterization of disease-associated mMED13L variants

We investigated a series of disease-associated MED13L variants, mMED13L-PL, -TM, -SL, -SY, and -Q*, as well as 2 general population variants -RQ(SNP) and -IV(SNP) *in vitro* (Fig. 3A). We began by investigating the potential effect of each variant on steady-state levels in over-expressing cells, as this biochemical feature is typically disrupted in disease-associated variants of protein-coding genes (Saitsu *et al.* 2010; Hamada *et al.* 2017; Noda *et al.* 2021; Hamada *et al.* 2021a). As shown, Western blotting revealed that mMED13L-Q* immunoblotted signal was weakly detected in lysates prepared from transiently transfected COS7 cells, while signals for other variants were comparable to wild type MED13L (WT) (Fig. 3B). We next examined the abundance and subcellular distribution of the variants over-expressed as myc-tagged constructs in electroporated cortical neurons *in vivo*. There, we found that myc-tagged immunostained mMED13L-Q* fluorescence signal was consistently weaker than in neurons transduced with myc-MED13L WT overexpression (Fig. 3C). In terms of subcellular localization of myc-tagged MED13L, we found that mMED13L-PL, -TM, mMED13L-RQ(SNP), and -IV(SNP) immunofluorescence signals were localized to the nucleus in a manner that was similar to mMED13L WT. In contrast, cells over-expressing mMED13L-SL and -SY displayed diffuse cytoplasmic immunofluorescence signal (Fig. 3C). It is noteworthy that disease-associated missense variants mapping to adjacent amino acid codons T2162 and S2163 have been reported to influence MED13L protein localization as well (Smol *et al.* 2018). Therefore, our expression assays *in vitro* and *in vivo* demonstrate that disease-associated MED13L missense variants influence steady state protein levels and subcellular localization in different ways.

Genetic variants of *MED13L* influence the dendritic development of cortical neurons

Given that our knockdown studies indicate that *MED13L* expression is necessary for dendritic arbor development, we explored the effects of our set of *MED13L* genetic variants in this feature for cortical neurons as well. Notably, as we find that mMED13L-Q* steady levels are visibly weaker than mMED13L WT in our over-expression assays with cortical neurons *in vivo* (Fig. 3B and C), one prediction is that its pathogenic impact may be reminiscent of MED13L haploinsufficiency (Yamamoto *et al.* 2017). In contrast, our overexpression studies found that the missense variants p.P866L, p.T2162M, p.S2163L, and p.S2177Y were localized within cortical neurons in different ways *in vivo*. Given that clinically-pathogenic *MED13L* variants are documented as heterozygous variations, we reasoned that each may interfere with the functions of wildtype MED13L. Thus, we explored the potential pathophysiological effects of these variants on dendritic development *in vivo*. Particularly, we investigated mMED13L-PL, -TM, and -SL for study because these variants are associated with neurodevelopmental abnormalities in humans, while we excluded mMED13L-SY because the clinical and molecular impact of an analogous mMED13L-SL variant has been reported (Smol *et al.* 2018).

We began by investigating the effect of the selected MED13L variants on cortical neuron migration and axon elongation during corticogenesis. As shown, *in utero* electroporation-mediated overexpression of mMED13L-PL, -TM, and -SL did not significantly influence the distribution of GFP-labelled neurons in cerebral cortex, nor influence axon elongation (Supplementary Fig. 3A and B). Next, we examined the potential effects of these variations on dendritic arbor development. As shown in Fig. 4, we found that the presence of mMED13L-PL

significantly impaired the dendritic arborization of cortical neurons, which suggests that p.P866L documented in humans may manifest as a dominant-negative variant *in vivo*. In contrast, we observed that the presence of mMED13L-SL in cortical neurons did not significantly influence dendritic arbor development (Fig. 4).

To further explore the effects of clinically relevant MED13L variants on dendritic development, we performed a series of rescue experiments in the context of mMED13L-knockdown. As shown, while electroporation of sh-mMED13L#1 of E14.5 cortical cells led to significant dendritic arborization effects in cortical neurons analyzed at P7, we found that this phenotype was rescued by co-treatment with mMED13L-R expression construct (Fig. 1C and Fig. 5A,a-c, and B). Under these conditions, mMED13L-TM exhibited moderate, statistically significant rescue of the defective basal dendrite length observed following mMED13L knockdown (Fig. 5A,d and B). In contrast, co-treatment with mMED13L-SL neither rescued nor enhanced the severity of basal dendritic length measurements in cortical neurons (Fig. 5A,e and B). These results suggest that the p.S2163L variant has no significant influence on dendritic arborization.

The MED13L-SL variant influences dendritic spine morphology *in vivo*

Given our previous finding that mMED13L is distributed at the synapses (Hamada *et al.* 2021b), and that impaired synaptic functions underlie the pathophysiology of ID (Batool *et al.* 2019; La Fata *et al.* 2014; Mancini *et al.* 2020), we next investigated the potential effects of the p.S2163L variant on spine density and morphogenesis of layer II-III cortical neurons *in vivo*. To do so, we examined dendritic spines on transduced cortical neurons in our experiments. Dendritic spines are the primary site of excitatory input, and their shape and size are critical for

the strength of excitatory synaptic connections. While we understand that dendritic spine shapes exist along a continuum, we nonetheless classified dendritic spine morphologies into 4 groups for our study as a methodological approach for quantification, as follows: mushroom-type spine represent mature spines, while stubby-, long thin-, and filopodia-type spines are classified as immature spines (Pchitskaya and Bezprozvanny 2020). To analyze spine morphologies, we electroporated wild type mMED13L or mMED13L-SL into VZ cells at E14.5, and brains were fixed and neurons analyzed at P30 (Fig. 6A and B). As shown in Fig. 6C, the cumulative density of dendritic spines was not statistically significant between WT and variant-expressing neurons. In contrast, expression of the variant led to a significant reduction in mushroom-type spine number, as well as an increase in the proportions of stubby-type spines (Fig. 6D). These results demonstrate that overexpression of a p.S2163L variant influences dendritic spine morphology, and could even disrupt the development and maintenance of functional synapses.

Discussion

The Mediator complex serves as a molecular interface that bridges signal transduction with target gene transcription within cells of the mammalian central nervous system, and disruptions to its function are associated with neuronal abnormalities. Genetic variations to the mediator complex subunit MED13L cause a clinical syndrome characterized by developmental delay, ID, speech impairment, and dysmorphic features, as well as autistic features, epilepsy, behavioral issues, and complex congenital heart defects (Asadollahi *et al.* 2013; Cafiero *et al.* 2015; van Haelst *et al.* 2015; Adegbola *et al.* 2015; Tørring *et al.* 2019). Given that the majority of reports describe *de novo* loss-of-function variations (Yamamoto *et al.* 2017), this condition has been

referred to as "MED13L haploinsufficiency syndrome". Furthermore, evidence of MED13L protein localization at neuronal synapses (Hamada *et al.* 2021b) indicates that it is relevant to the functions of the nervous system.

It is recognized that variations in Mediator subunit genes cause neurodevelopmental disorders, yet the underlying molecular mechanisms have been described in anecdotal cases. For example, the *MED12* p.R961W and p.N1007S variants associated with Opitz–Kaveggia syndrome and Lujan–Fryns syndrome, respectively, were documented to disrupt the molecular interaction of MED12 with the transcription repressor known as REST (Ding *et al.* 2008). In another study, the p.R617Q missense variant for *MED23* associated with non-syndromic autosomal recessive ID was reported to impair the molecular functions of this protein to transcription factors JUN and FOS (Hashimoto *et al.* 2011; Khattak and Mir 2014). In this study, we have found that mMED13L influences dendrite growth during corticogenesis *in vivo*. Furthermore, our studies of mouse orthologues for 5 disease-associated MED13L missense variants detected in humans revealed a spectrum of neuronal phenotypes *in vivo* and *in vitro,* which we predict will be informative to our understanding of the clinical heterogeneity of MED13L syndrome. For example, our characterization studies of the mMED13L-Q* found that steady-state levels of this variant, compared to the wild type, is significantly lower in COS7 cells and in cortical neurons. As such, these results are consistent with the report that the p.Q1922* variant in humans manifests as a clinical haploinsufficiency phenotype. Furthermore, our mMED13L-knockdown studies are also consistent with the notion that *MED13L* suppression disrupts neuronal development through direct effects on developing cortical neurons.

In our case of studies with mMED13L-SL and -SY variants that are associated with severe clinical symptoms, we observed that myc-tagged versions of these proteins distributed diffusely in the cytoplasm of cortical neurons, in contrast to wild type mMED13L that was localized to the nucleus. It is notable that we also found that the missense MED13L variants in healthy individuals localized to the nucleus in a manner that was non significantly different to the wild type. The Mediator complex is recognized to localize to the nucleus to carry out its functions within cells, and so the presence of the missense variants mMED13L-SL and -SY may disrupt MED13L incorporation within the complex, subcellular localization of the complex, or both. Furthermore, these variants may even bind non-native molecules within cells that explain their retention within the cytoplasm. Nevertheless, the molecular mechanisms for this phenotype and how it relates to the clinical severity of MED13L syndrome remains unclear. However, we believe that nuclear localization is critical to MED13L functions in neurons, since we find that the mMED13L-TM variant, which is nuclear localized, could partially rescue the dendritic growth defects of mMED13L-knockdown cortical neurons. We thus interpret this result to suggest that the presence of the orthologous human MED13L variant p.T2162M could lead to impaired MED13L function, rather than haploinsufficiency. In contrast, we found that mMED13L-PL was localized to the nucleus of cortical neurons (Fig. 3) and its overexpression disrupted dendritic arborization (Fig. 4), which collectively indicated that the orthologous human variant p.P866L could exert a dominant effect as a heterozygous mutation. Taken altogether, our findings provide insight into potential molecular and cellular effects of MED13L variants on the clinical heterogeneity of MED13L syndrome (Table 1).

Beyond their genotype-phenotype association with neurological phenotypes, variations to Mediator subunit genes are also associated with transposition of the great arteries and congenital heart disease (Muncke *et al.* 2003; Grueter 2013). Furthermore, expression levels of Mediator subunits are correlated with cancer. For example, overexpression of *MED23* is significantly correlated with lung cancer associated with enhanced *RAS* oncogene activity, while weak *MED23* expression is associated with survival (Yang *et al.* 2012). Also, *MED15* is highly expressed in breast cancer tissues and is linked to hyperactivation of the transforming growth factor β (TGFβ)-mediated signaling pathway, while *MED15* deficiency led to a decrease in the metastatic potential of breast cancer cells through attenuation of TGFβ signaling (Zhao *et al.* 2013). In another example, heterozygous variants in *MED12* have been frequently described in uterine leiomyomas (Mäkinen *et al.* 2011). From these observations, we find that Mediator genes are involved in tissue carcinogenesis and metastasis through multiple signaling pathways. Hyperactivation (gain-of-function) of the Mediator complex could potentiate carcinogenesis, while loss-of-function, neofunctionalization (i.e. gain-of-pathological-function) or dominant-negative mechanisms for Mediator genes may relevant to neuropathological states.

A significant limitation of our study is related to our *in utero* electroporation-mediated gene transfer approach with mouse embryos. We appreciate that our findings in mice may not recapitulate the functions for MED13L in human neurons. Furthermore, we understand that the stochastic effects of gene transfection *in vivo* are also limited by physical constraints of the embryonic cortical VZ, the features of transduced cells and our surgical protocol. Nevertheless, our knockdown experiments are consistent with the notion that appropriate levels of MED13L are required for cortical dendrite development, and we believe these results provide insight into

the effect of *MED13L* haploinsufficiency in humans. Equally, our overexpression studies have provided an opportunity to appreciate the potential effects of heterozygous *MED13L* variants that underlie human neurodevelopmental phenotypes.

In conclusion, our study provides evidence that MED13L is relevant to mammalian neurodevelopment through its functions in influencing the dendritic development and synaptic spine features of excitatory neurons of the cerebral cortex. Furthermore, we find that disease-associated variants of MED13L exert their effects in different ways.

Human subjects:

Involves human subjects:

If yes: Informed consent & ethics approval achieved:

if yes, please ensure that the info "Informed consent was achieved for all subjects, and the experiments were approved by the local ethics committee." is included in the Methods.

Acknowledgments:

This work was funded by Japan Society for the Promotion of Science, (Grant / Award Number: 'JP19H03629','JP19K07059','JP20K21589')

Japan Agency for Medical Research and Development, (Grant / Award Number: '15ek0109040h0002') (grant number): This information is usually included already, but please add to the Acknowledgments if not.

Author contributions

ARRIVE guidelines have been followed:

Yes

if it is a Review or Editorial, skip complete sentence

if No, include a statement in the "Conflict of interest disclosure" section: "ARRIVE guidelines were not followed for the following reason:

"

(edit phrasing to form a complete sentence as necessary).

if Yes, insert in the "Conflict of interest disclosure" section:

"All experiments were conducted in compliance with the ARRIVE guidelines." unless it is a Review or Editorial

Conflicts of interest: none

if 'none', insert "The authors have no conflict of interest to declare."

else insert info unless it is already included

Acknowledgements

We thank Ms. Hiroko Kosuge for technical assistance. Manuscript editor Dr. Julian Heng (REMOTELY CONSULTING) provided professional English-language editing of this article.

Competing Financial Interests statement

The authors declare no competing financial interests.

Author Contribution

NH designed and made RNAi- and expression-vectors, carried out *in utero* electroporation and immunohistochemical analyses, and helped to draft the manuscript. II carried out biochemical analyses. KN conceived of the study, participated in its design and coordination, and drafted the manuscript. All authors read and approved the final manuscript.

Funding Sources

This work was supported in part by Japan Society for the Promotion of Science (JSPS) KAKENHI Grant-in-Aid for Scientific Research (B) (Grant Number JP19H03629), Grant-in-Aid for Scientific Research (C) (Grant Number JP19K07059), Grant-in-Aid for Challenging Research (Pioneering/Exploratory) (Grant Number JP20K21589), and a grant-in-aid of the Practical Research Project for Rare/Intractable Diseases from Japan Agency for Medical Research and Development (AMED) (15ek0109040h0002).

Figure legends

Figure 1. Characterization of MED13L in COS7 cells and cortical neurons *in vivo*

(A) pSuper-mMED13L#1 and #2, and pCAG-Myc-mMED13L-R. pCAG-Myc-mMED13L or Myc-mMED13L-R was co-transfected into COS7 cells, in combination with control pSuper-H1.shLuc (pSuper), pSuper-mMED13L (sh-mMED13L) #1or #2, as shown. After 48 h, cells

were harvested and subjected to western blotting with anti-Myc. Immunoblotting of the cytoskeleton-related protein, Sept11, was used for loading control. Relative levels of Myc-mMED13L and -mMED13L-R were calculated with ImageJ software based on densitometry and normalized against Sept11. Error bars indicate SD [n = 3 (n = number of independent cell culture preparations)]. ****$P < 0.0001$ by one-way ANOVA < with Tukey's LSD post hoc test. **(B)** Knockdown of endogenous mMED13L in primary cultured cortical neurons. pCAG-EGFP (0.1 μg) was transfected with pSuper-H1.shLuc (control), sh-mMED13L#1 or #2 (0.5 μg each) into E14.5-born cortical neurons and dissociated at E16.5. Cells were then cultured for 48 h, fixed and immunostained with anti-MED13L (red) and DAPI (blue). Knockdown cells are marked by *arrowheads*. Scale bar, 10 μm. **(C)** Effects of mMED13L-knockdown on dendritic growth *in vivo*. pCAG-loxP-GFP (0.5 μg) was co-electroporated with pCAG-M-Cre (0.5 ng) for sparse expression together with pSuper-H1.shLuc (1.0 μg, control), sh-mMED13L#1 or #2 (1 μg each) with pCAG-Myc (0.3 μg), or sh-mMED13L#1 + pCAG-Myc-mMED13L-R (0.3 μg) at E14.5. Coronal sections were prepared with brains collected at P7, then immunostained for GFP and analyzed. Representative average *z*-stack projection images of layer II/III cortical neurons are shown. Scale bar, 10 μm. (**D**) Total length was calculated for apical and basal dendrites in (C). ***$P < 0.001$ and ****$P < 0.0001$ by one-way ANOVA with Tukey's *post hoc* test. **(E)** Branch points of dendrites in (C) were quantified by Sholl analysis. Five sections from each brain were analyzed [n= number of animals. control (n=5), sh-mMED13L#1 (n=5), sh-mMED13L#2 (n=3), and sh-mMED13L#1 + pCAG-Myc-mMED13L-R (n=4)]. Error bars indicate SD of the results from 15 to 26 neurons. Statistical analysis was performed in the area within 30 μm distance from soma. **$p< 0.01$ and ****$P < 0.0001$ by Tukey-Kramer LSD. The

box dimensions indicate from the 25th to 75th percentiles, and line indicates the median. The whiskers indicate the largest/lowest points.

Figure 2. The effect of mMED13L-knockdown on dendrite growth in postnatal (P30) cortical neurons *in vivo*

(**A**) pCAG-loxP-GFP (0.5 μg) was co-electroporated with pCAG-M-Cre (0.5 ng) for sparse expression together with pSuper-H1.shLuc (1.0 μg, control) or sh-mMED13L#1 (1 μg) at E14.5. After fixation at P30, coronal sections were prepared and stained for GFP. Representative average *z*-stack projection images of layer II/III cortical neurons were shown. Scale bar, 20 μm. (**B** and **C**) Number and total length of basal dendrites in (A) were quantified (B). Branch points of basal dendrites in (A) were analyzed by Sholl analysis (C). Five sections from each brain were analyzed (n= number of animals. control, n=5; KD #1, n=6). Error bars indicate SD of the results from 29 to 36 neurons; ***$P < 0.001$ and ****$P < 0.0001$ by Welch's t-test. The box dimensions indicate from the 25th to 75th percentiles, and line indicates the median. The whiskers indicate the largest/lowest points.

Figure 3. Stability and subcellular localization of disease-associated *MED13L* variants

(A) Schematic representation of human MED13L with genetic variants analyzed [24], in conjunction with orthologous variants in mouse polypeptide sequence. Clinical variants associated with severe and mild phenotypes were shown in red and yellow, respectively. General population missense variants are identified in blue text. **(B)** Expression of Myc-tagged mMED13L (WT), -mMED13L-RQ (SNP), -IV (SNP) and variants (mMED13L-PL, -Q*, -TM,

-SL and -SY) in COS7 cells. Forty-eight hours after transfection, cells were harvested and subjected to western blotting with anti-Myc antibody. β–actin immunoblotting was carried out as loading control. **(C)** Overexpression of mMED13L and genetic variants in developing cortical neurons *in vivo*. pCAG-EGFP (0.1 μg) was co-electroporated into the VZ progenitors at E14.5 with 0.5 μg each of pCAG-Myc-mMED13L, -mMED13L-RQ(SNP), -IV(SNP), -PL, -Q*, -TM, -SL or -SY followed by collection at P2 for processing, cryosectioning, immunostaining and fluorescence microscopy. Coronal sections were stained for GFP (white) and Myc-tag (magenta). Scale bar, 5 μm.

Figure 4. Disease-associated *MED13L* variants influence the dendritic development of layer II/III cortical neurons *in vivo*

(A) For sparse expression, pCAG-loxP-GFP (0.5 μg) was co-electroporated with pCAG-M-Cre (0.5 ng) together with pCAG-Myc-mMED13L (WT), -RQ (healthy SNP), -PL, -TM or -SL (1 μg each) at E14.5. Analyses were carried out as per described for Fig. 1C. Scale bar, 20 μm. Expression of Myc-mMED13L (WT), -mMED13L-PL, -TM and -SL were visualized by staining for Myc-tag (magenta) **(B)** Total basal dendrite length was calculated on neurons observed in (A). Five sections from each brain were analyzed (n= number of animals. WT, n=5; PL, n=5; TM, n=5; SL, n=4). Error bars indicate SD of the results from 21 to 28 neurons. ***$p<$ 0.001 by Tukey-Kramer LSD. The box dimensions indicate from the 25th to 75th percentiles, and line indicates the median. The whiskers indicate the largest/lowest points. **(C)** Branch points of dendrites in (A) were quantified by Sholl analysis. Five sections from each brain were analyzed (n= number of animals. WT, n=3; PL, n=3; TM, n=3; SL, n=3). Error bars indicate SD

of the results from 15 to 26 neurons. Statistical analysis was performed in the area within 30 μm distance from soma. ***p< 0.001 and ****P < 0.0001 by Tukey-Kramer LSD.

Figure 5. The effects of mMED13L-TM and -SL genetic rescue on defective dendritic growth following mMED13L-knockdown *in vivo*

(A) pCAG-loxP-GFP (0.5 μg) was co-electroporated with pCAG-M-Cre (0.5 ng) together with pSuper-H1.shLuc (Control), sh-mMED13L#1 + pCAG-Myc (vector), sh-mMED13L#1 + pCAG-Myc-mMED13L-WT (WT-#1R) or each variant expression vector (1 μg each of pSuper vector and 0.3 μg each of pCAG vector) into VZ progenitor cells at E14.5. Analyses were carried out as per described in Fig. 1C. Scale bar, 20 μm. **(B)** Total basal dendritic length was calculated on neurons observed in (A). Five sections from each brain were analyzed (n= number of animals. Control, n=5; vector, n=3; WT-#1R, n=4; TM-#1R, n=5; SL-#1R, n=5). Error bars indicate SD of the results from 15 to 24 neurons. *p< 0.05 and ****p< 0.0001 by Tukey-Kramer LSD. The box dimensions indicate from the 25th to 75th percentiles, and line indicates the median. The whiskers indicate the largest/lowest points.

Figure 6. The effects of overexpressing wildtype MED13L and mMED13L-SL on dendritic spine features on postnatal (P30) cortical neurons

(**A** and **B**) pCAG-loxP-GFP (0.5 μg) was co-electroporated for sparse expression with pCAG-M-Cre (0.5 ng) together with pCAG-Myc-mMED13L (WT) or -mMED13L-SL (1 μg each) at E14.5. Coronal sections were prepared at P30 and stained for GFP (A). Representative images of dendritic spines on the 1st-order apical dendrites were shown (B). Note that the cell shape at

P30 was different from that at P7 (Fig. 1C). Scale bars, 20 μm (A) and 5 μm (B). (**C - D**) Quantitative analyses of spine density (C) and spine morphology (mushroom-type, stubby, long thin and filopodia-like spines) (D) in layer II/III excitatory neurons. One section from each brain was analyzed (n= number of animals. WT, n=4; SL, n=5). Error bars indicate SD of the results from 6 (WT) and 9 (SL) neurons by Welch's t-test. *$p < 0.05$ and **$p < 0.01$. The box dimensions indicate from the 25th to 75th percentiles, and line indicates the median. The whiskers indicate the largest/lowest points.

Table 1. Schematic summary of the pathogenic impact of MED13L variants.

References

Adegbola A., Musante L., Callewaert B., Maciel P., Hu H., Isidor B., Picker-Minh S., et al. (2015) Redefining the MED13L syndrome. *European Journal of Human Genetics* **23**, 1308–1317.

Asadollahi R., Oneda B., Sheth F., Azzarello-Burri S., Baldinger R., Joset P., Latal B., et al. (2013) Dosage changes of MED13L further delineate its role in congenital heart defects and intellectual disability. *European Journal of Human Genetics* **21**, 1100–1104.

Batool S., Raza H., Zaidi J., Riaz S., Hasan S., Syed N. I. (2019) Synapse formation: from cellular and molecular mechanisms to neurodevelopmental and neurodegenerative disorders. *J Neurophysiol* **121**, 1381–1397.

Berti L., Mittler G., Przemeck G. K., Stelzer G., Günzler B., Amati F., Conti E., et al. (2001) Isolation and characterization of a novel gene from the DiGeorge chromosomal region that encodes for a mediator subunit. *Genomics* **74**, 320–332.

Boutry-Kryza N., Labalme A., Till M., Schluth-Bolard C., Langue J., Turleau C., Edery P., Sanlaville D. (2012) An 800 kb deletion at 17q23.2 including the MED13 (THRAP1) gene, revealed by aCGH in a patient with a SMC 17p. *Am. J. Med. Genet.* **158A**, 400–405.

Bulayeva K., Lesch K.-P., Bulayev O., Walsh C., Glatt S., Gurgenova F., Omarova J., Berdichevets I., Thompson P. M. (2015) Genomic structural variants are linked with intellectual disability. *J Neural Transm* **122**, 1289–1301.

Cafiero C., Marangi G., Orteschi D., Ali M., Asaro A., Ponzi E., Moncada A., et al. (2015) Novel de novo heterozygous loss-of-function variants in MED13L and further delineation of the MED13L haploinsufficiency syndrome. *European Journal of Human Genetics* **23**, 1499–1504.

Casamassimi A., Napoli C. (2007) Mediator complexes and eukaryotic transcription regulation: an overview. *Biochimie* **89**, 1439–1446.

Ding N., Zhou H., Esteve P.-O., Chin H. G., Kim S., Xu X., Joseph S. M., et al. (2008) Mediator links epigenetic silencing of neuronal gene expression with x-linked mental retardation. *Mol Cell* **31**, 347–359.

Gordon C. T., Chopra M., Oufadem M., Alibeu O., Bras M., Boddaert N., Bole-Feysot C., et al. (2018) MED13L loss-of-function variants in two patients with syndromic Pierre Robin sequence. *Am. J. Med. Genet.* **176**, 181–186.

Grueter C. E. (2013) Mediator complex dependent regulation of cardiac development and disease. *Genomics Proteomics Bioinformatics* **11**, 151–157.

Hamada N., Iwamoto I., Kawamura N., Nagata K.-I. (2021a) Heterotrimeric G-protein, Gi1, is involved in the regulation of proliferation, neuronal migration, and dendrite morphology during cortical development in vivo. *J. Neurochem.* **157**, 1167–1181.

Hamada N., Iwamoto I., Nishikawa M., Nagata K.-I. (2021b) Expression Analyses of Mediator Complex Subunit 13-Like: A Responsible Gene for Neurodevelopmental Disorders during Mouse Brain Development. *Dev. Neurosci.* **43**, 43–52.

Hamada N., Ogaya S., Nakashima M., Nishijo T., Sugawara Y., Iwamoto I., Ito H., et al. (2018) De novo PHACTR1 mutations in West syndrome and their pathophysiological effects. *Brain* **141**, 3098–3114.

Hamada N., Iwamoto I., Tabata H., Nagata K.-I. (2017) MUNC18–1 gene abnormalities are involved in neurodevelopmental disorders through defective cortical architecture during brain development. *Acta Neuropathologica Communications*, 1–16.

Hamada N., Negishi Y., Mizuno M., Miya F., Hattori A., Okamoto N., Kato M., et al. (2016) Role of a heterotrimeric G-protein, Gi2, in the corticogenesis: possible involvement in periventricular nodular heterotopia and intellectual disability. *J. Neurochem.* **140**, 82–95.

Matsumura K., Seiriki K., Okada S., Nagase M., Ayabe S., Yamada I., Furuse T., et al. (2020) Pathogenic POGZ mutation causes impaired cortical development and reversible autism-like phenotypes. *Nature Communications* 11, 1–16.

Muncke N., Jung C., Rüdiger H., Ulmer H., Roeth R., Hubert A., Goldmuntz E., et al. (2003) Missense mutations and gene interruption in PROSIT240, a novel TRAP240-like gene, in patients with congenital heart defect (transposition of the great arteries). *Circulation* **108**, 2843–2850.

Noda M., Ito H., Nagata K.-I. (2021) Physiological significance of WDR45, a responsible gene for β-propeller protein associated neurodegeneration (BPAN), in brain development. *Scientific reports*, 1–14.

Pchitskaya E., Bezprozvanny I. (2020) Dendritic Spines Shape Analysis-Classification or Clusterization? Perspective. *Front Synaptic Neurosci* **12**, 31.

Pescosolido M. F., Gamsiz E. D., Nagpal S., Morrow E. M. (2013) Distribution of disease-associated copy number variants across distinct disorders of cognitive development. *J Am Acad Child Adolesc Psychiatry* **52**, 414–430.e14.

Risheg H., Graham J. M., Clark R. D., Rogers R. C., Opitz J. M., Moeschler J. B., Peiffer A. P., et al. (2007) A recurrent mutation in MED12 leading to R961W causes Opitz-Kaveggia syndrome. *Nat. Genet.* **39**, 451–453.

Roustan A., Perrin J., Berthelot-Ricou A., Lopez E., Botta A., Courbiere B. (2012) Evaluating methods of mouse euthanasia on the oocyte quality: cervical dislocation versus isoflurane inhalation. *Lab. Anim.* **46**, 167–169.

Saitsu H., Kato M., Okada I., Orii K. E., Higuchi T., Hoshino H., Kubota M., et al. (2010) STXBP1 mutations in early infantile epileptic encephalopathy with suppression-burst pattern. *Epilepsia* **51**, 2397–2405.

Schwartz C. E., Tarpey P. S., Lubs H. A., Verloes A., May M. M., Risheg H., Friez M. J., et al. (2007) The original Lujan syndrome family has a novel missense mutation (p.N1007S) in the MED12 gene. *J. Med. Genet.* **44**, 472–477.

Smol T., Petit F., Piton A., Keren B., Sanlaville D., Afenjar A., Baker S., et al. (2018) MED13L-related intellectual disability: involvement of missense variants and delineation of the phenotype. *Neurogenetics* **19**, 1–11.

Taatjes D. J. (2010) The human Mediator complex: a versatile, genome-wide regulator of transcription. *Trends Biochem. Sci.* **35**, 315–322.

Hanai N., Nagata K.-I., Kawajiri A., Shiromizu T., Saitoh N., Hasegawa Y., Murakami S., Inagaki M. (2004) Biochemical and cell biological characterization of a mammalian septin, Sept11. *FEBS Lett.* **568**, 83–88.

Hashimoto S., Boissel S., Zarhrate M., Rio M., Munnich A., Egly J.-M., Colleaux L. (2011) MED23 mutation links intellectual disability to dysregulation of immediate early gene expression. *Science* **333**, 1161–1163.

Kaufmann R., Straussberg R., Mandel H., Fattal-Valevski A., Ben-Zeev B., Naamati A., Shaag A., et al. (2010) Infantile cerebral and cerebellar atrophy is associated with a mutation in the MED17 subunit of the transcription preinitiation mediator complex. *Am. J. Hum. Genet.* **87**, 667–670.

Kawai S., Takagi Y., Kaneko S., Kurosawa T. (2011) Effect of three types of mixed anesthetic agents alternate to ketamine in mice. *Exp. Anim.* **60**, 481–487.

Khattak N. A., Mir A. (2014) Computational analysis of TRAPPC9: candidate gene for autosomal recessive non-syndromic mental retardation. *CNS Neurol Disord Drug Targets* **13**, 699–711.

La Fata G., Gärtner A., Domínguez-Iturza N., Dresselaers T., Dawitz J., Poorthuis R. B., Averna M., et al. (2014) FMRP regulates multipolar to bipolar transition affecting neuronal migration and cortical circuitry. *Nature Publishing Group* **17**, 1693–1700.

Leal A., Huehne K., Bauer F., Sticht H., Berger P., Suter U., Morera B., et al. (2009) Identification of the variant Ala335Val of MED25 as responsible for CMT2B2: molecular data, functional studies of the SH3 recognition motif and correlation between wild-type MED25 and PMP22 RNA levels in CMT1A animal models. *Neurogenetics* **10**, 375–376.

Liu X., Bushnell D. A., Kornberg R. D. (2013) RNA polymerase II transcription: structure and mechanism. *Biochim. Biophys. Acta* **1829**, 2–8.

Malik S., Roeder R. G. (2010) The metazoan Mediator co-activator complex as an integrative hub for transcriptional regulation. *Nat Rev Genet* **11**, 761–772.

Mancini M., Bassani S., Passafaro M. (2020) Right Place at the Right Time: How Changes in Protocadherins Affect Synaptic Connections Contributing to the Etiology of Neurodevelopmental Disorders. *Cells* **9**, 2711.

Mäkinen N., Mehine M., Tolvanen J., Kaasinen E., Li Y., Lehtonen H. J., Gentile M., et al. (2011) MED12, the mediator complex subunit 12 gene, is mutated at high frequency in uterine leiomyomas. *Science* **334**, 252–255.

Tabata H., Nakajima K. (2001) Efficient in utero gene transfer system to the developing mouse brain using electroporation: visualization of neuronal migration in the developing cortex. *Neuroscience* **103**, 865–872.

Tørring P. M., Larsen M. J., Brasch-Andersen C., Krogh L. N., Kibæk M., Laulund L., Illum N., et al. (2019) Is MED13L-related intellectual disability a recognizable syndrome? *European Journal of Medical Genetics* **62**, 129–136.

van Haelst M. M., Monroe G. R., Duran K., van Binsbergen E., Breur J. M., Giltay J. C., van Haaften G. (2015) Further confirmation of the MED13L haploinsufficiency syndrome. *European Journal of Human Genetics* **23**, 135–138.

Yamamoto T., Shimojima K., Ondo Y., Shimakawa S., Okamoto N. (2017) MED13L haploinsufficiency syndrome: A de novo frameshift and recurrent intragenic deletions due to parental mosaicism. *Am. J. Med. Genet.* **173**, 1264–1269.

Yang X., Zhao M., Xia M., Liu Y., Yan J., Ji H., Wang G. (2012) Selective requirement for Mediator MED23 in Ras-active lung cancer. *Proc. Natl. Acad. Sci. U.S.A.* **109**, E2813–22.

Zhao M., Yang X., Fu Y., Wang H., Ning Y., Yan J., Chen Y.-G., Wang G. (2013) Mediator MED15 modulates transforming growth factor beta (TGFβ)/Smad signaling and breast cancer cell metastasis. *J Mol Cell Biol* **5**, 57–60.

Table 1. Summary of the effects of pathogenic MED13L variants

	Dendritogenesis (Variation type)	Synaptogenesis (Variation type)	Location	Clinical feature
P866L	✕ (GoF or DN)	ND	Nuc	ID + ASD + seizure + hypotonia
S2163L	✕ (LoF)	✕ (GoF)	Cyt	
T2162M	△ (RoF)	ND	Nuc	ID only
Q1922*	✕ (LoF)	ND	(-)	

△, partially impaired; X, impaired; ND, not determined; Nuc, nucleus; Cyt, cytoplasm;
GoF, Gain-of-pathological-function; DN, dominant negative; LoF, Loss-of-function;
RoF, Reduction-of-function

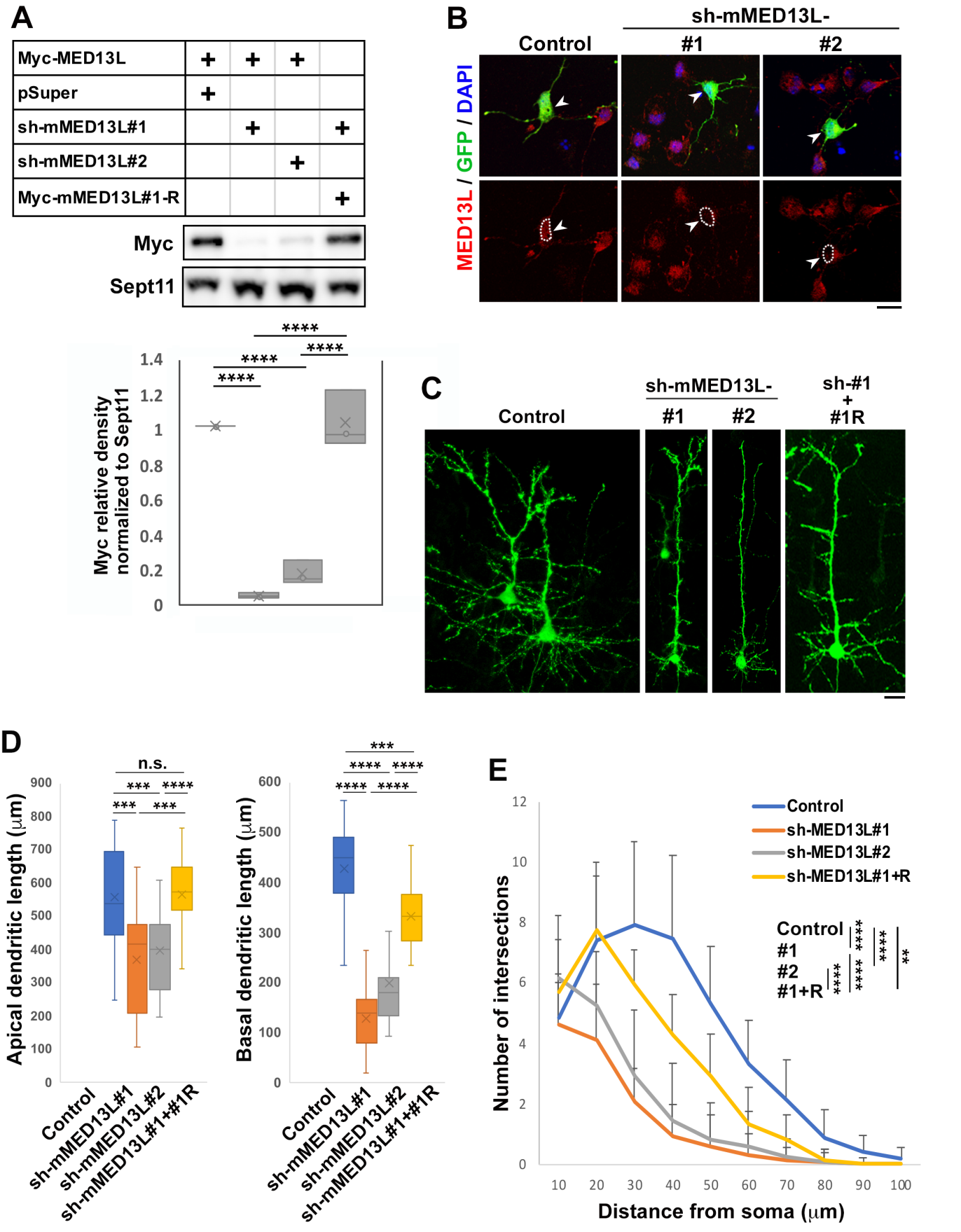

Figure 1. Hamada et al.

JNC_15783_Fig1.tif

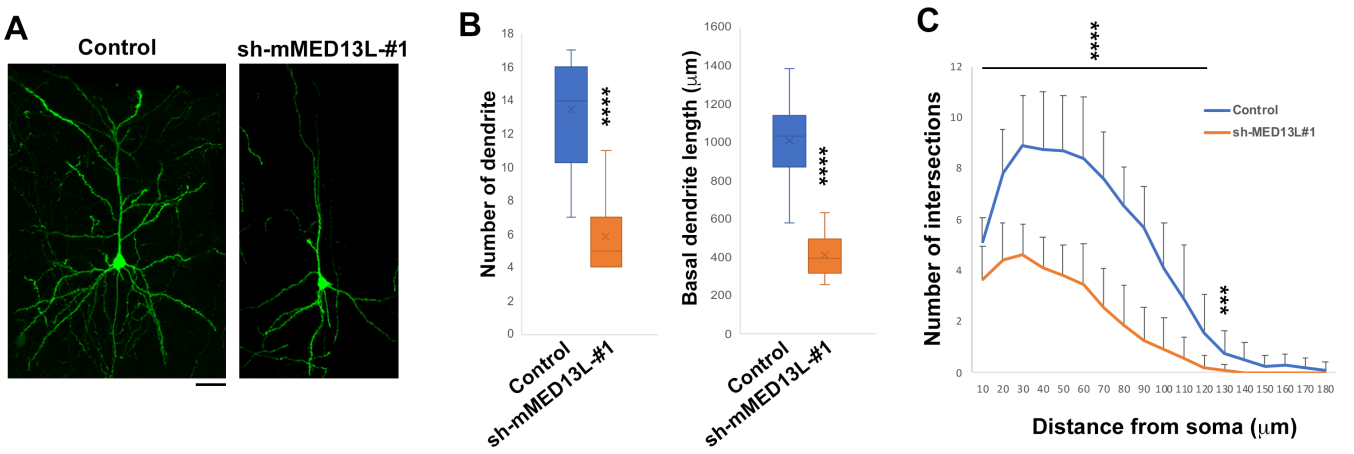

Figure 2. Hamada et al.

JNC_15783_Fig2.tif

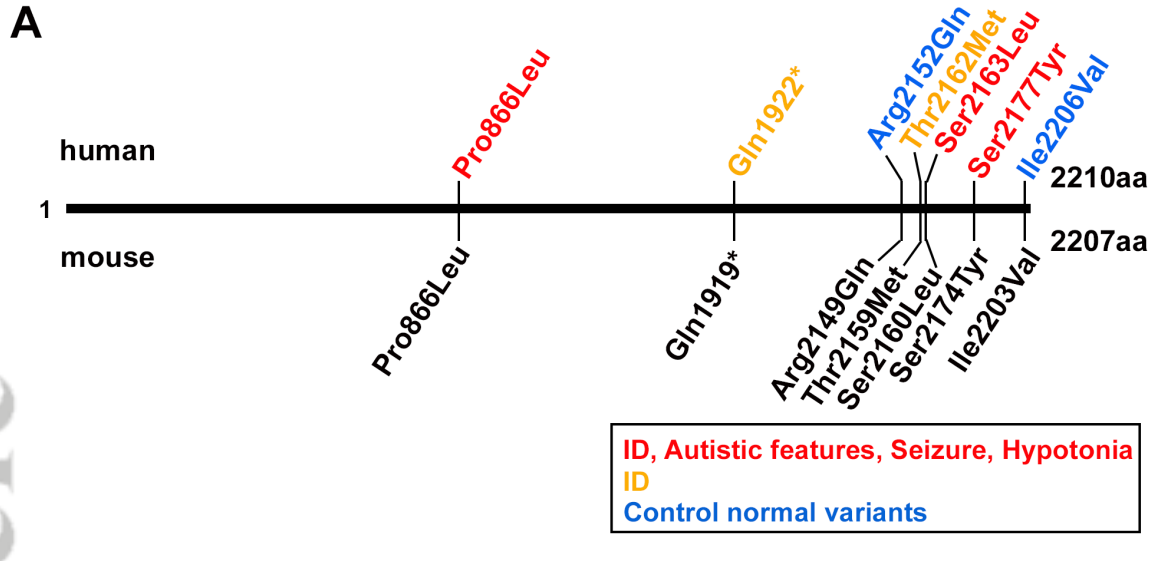

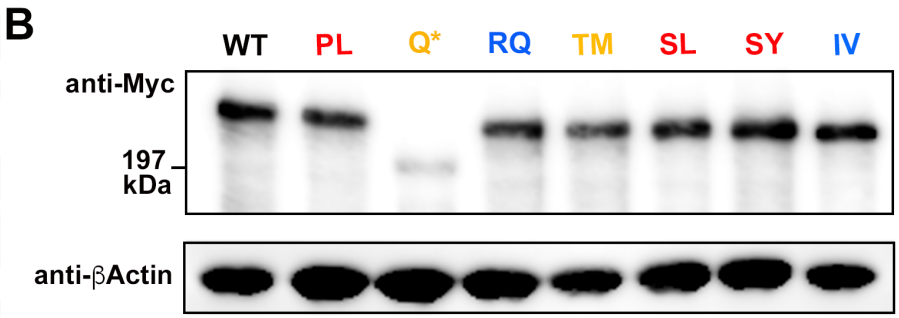

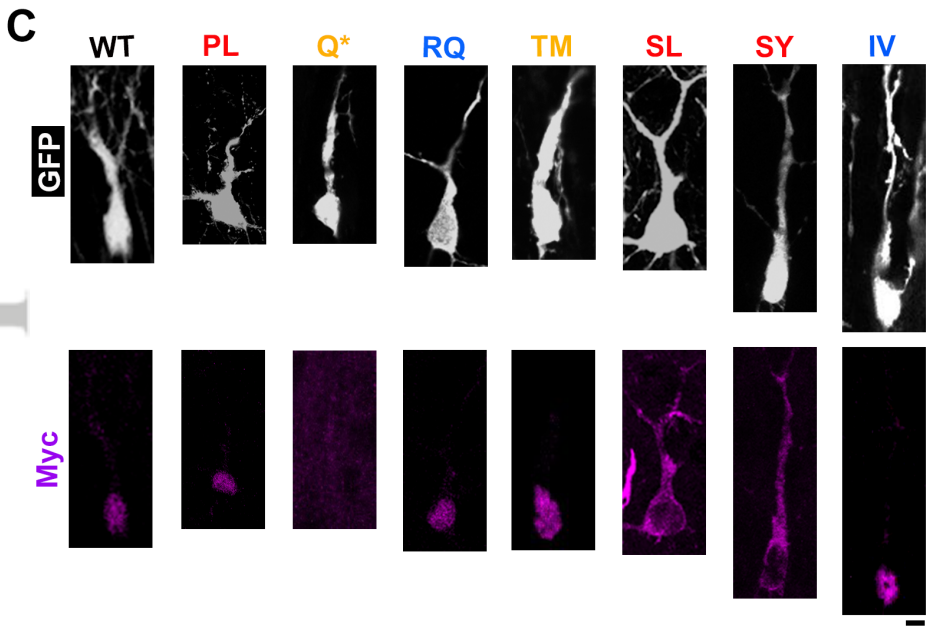

Figure 3. Hamada et al.

JNC_15783_Fig3.tif

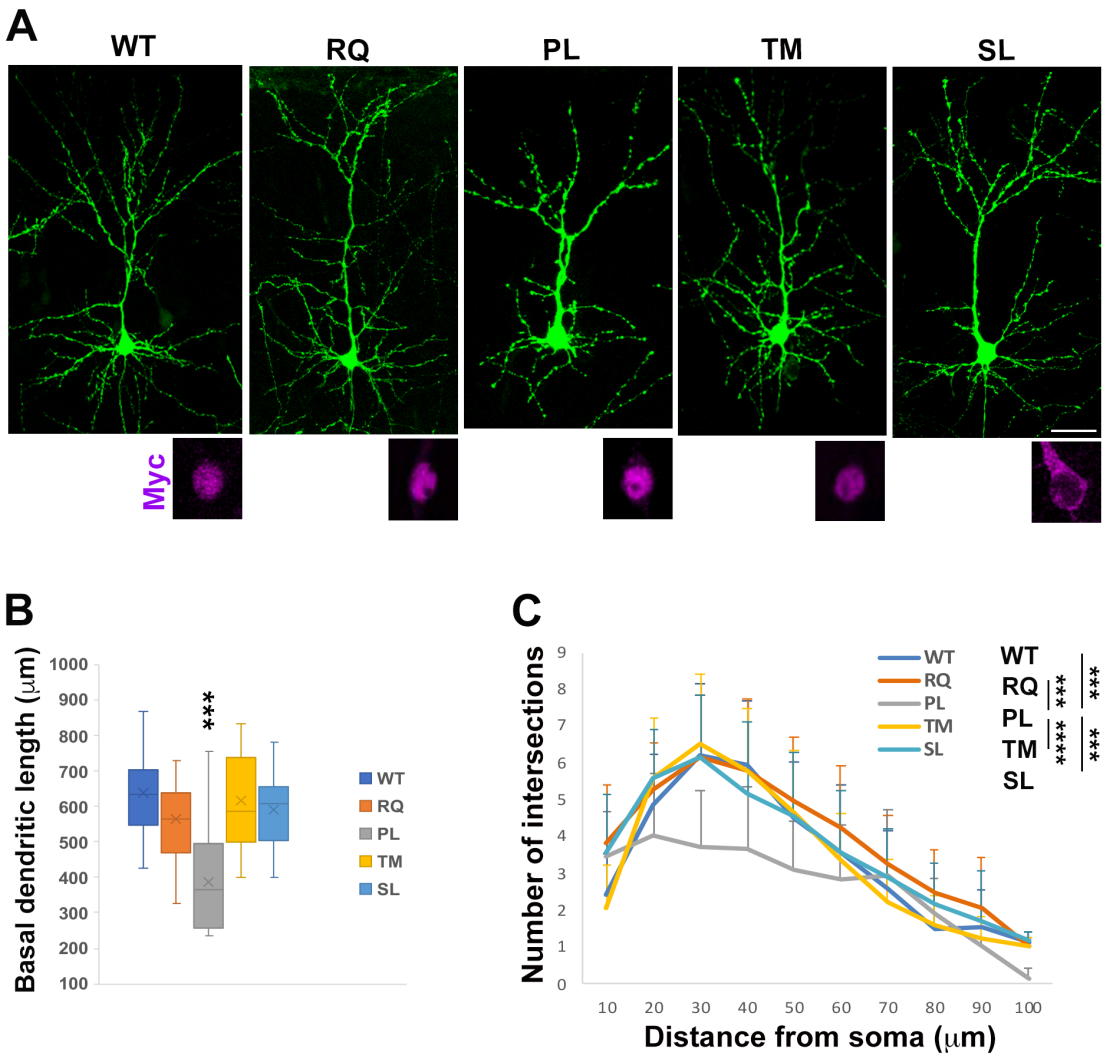

Figure 4. Hamada et al.

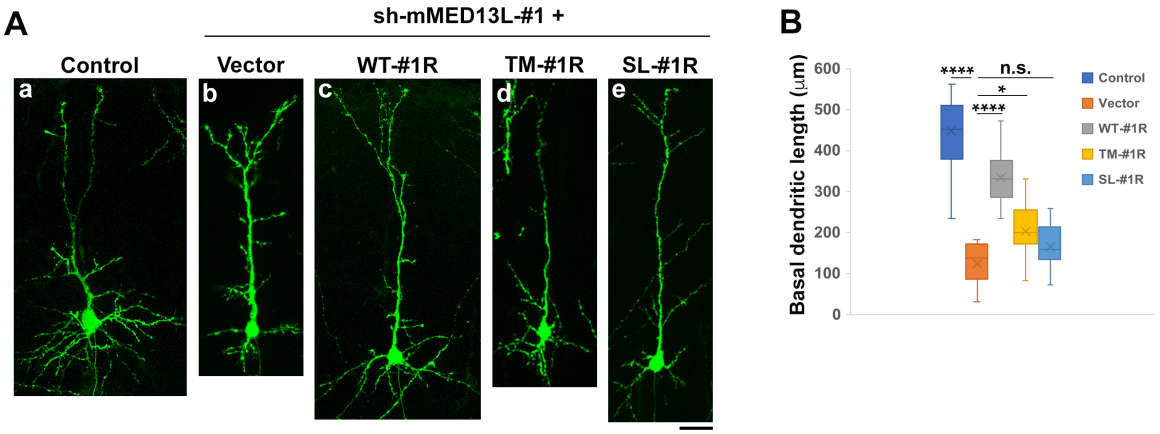

Figure 5. Hamada et al.

JNC_15783_Fig5.tif

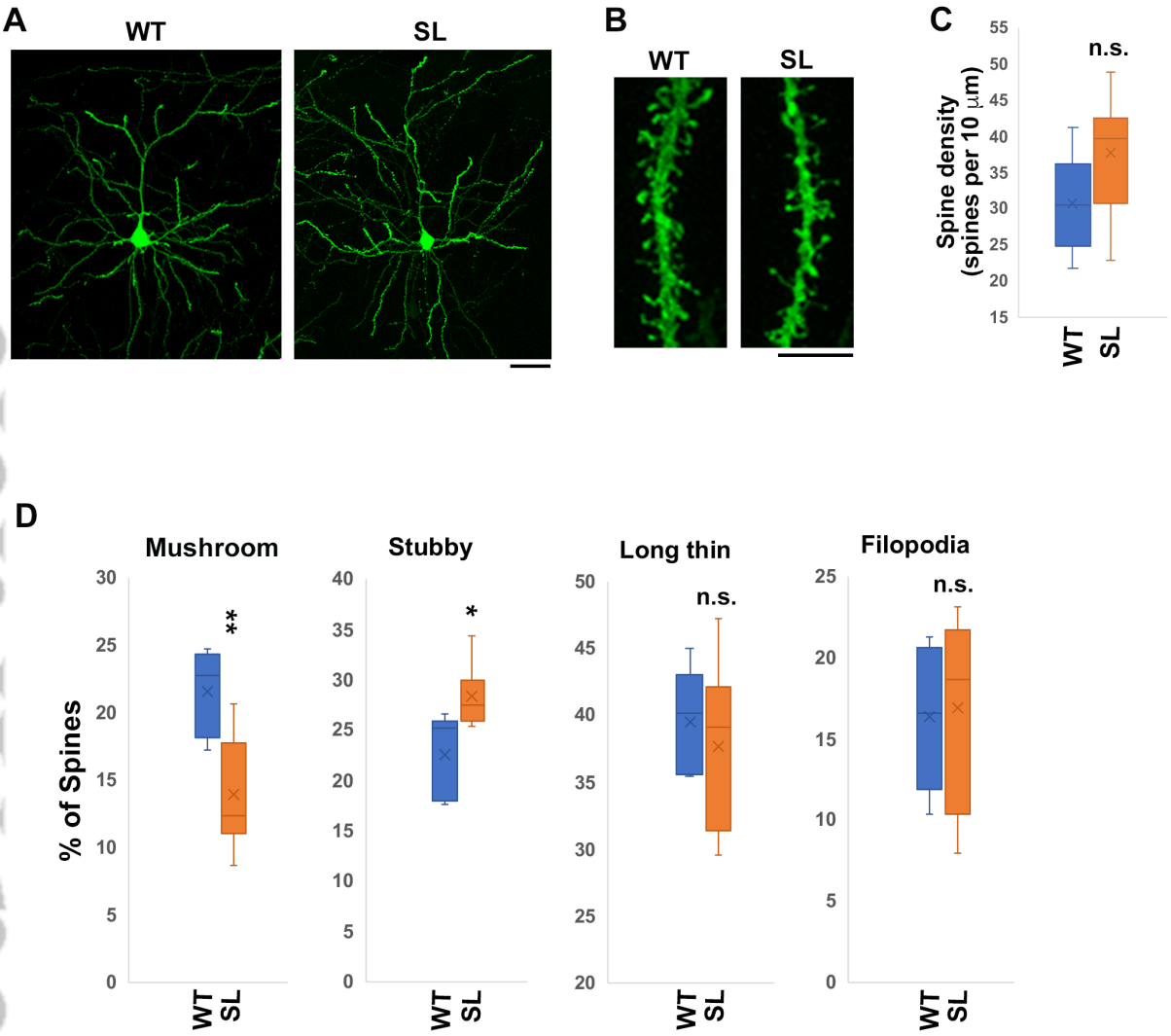

Figure 6. Hamada et al.

JNC_15783_Fig6.tif